ICARUS **133,** 310–320 (1998)
ARTICLE NO. IS985938

# Size Dependence of Restitution Coefficients of Ice in Relation to Collision Strength

Michiya Higa,[1] Masahiko Arakawa, and Norikazu Maeno

*Institute of Low Temperature Science, Hokkaido University, Kita-ku Kita-19 Nishi-8, Sapporo 060, Japan*
E-mail: higa@planeta.sci.isas.ac.jp

Received May 12, 1997; revised April 1, 1998

**We have investigated the size dependence of the restitution coefficient ($\varepsilon$) of a water ice sphere over a wide range of impact velocities ($v_i$ = 1–1000 cm/s) and radii ($r_p$ = 0.14–3.6 cm) at 261 K. The impact velocity dependence of $\varepsilon$ was divided into two regions by the critical velocity ($v_c$), which was the onset velocity of fracturing as well. In the quasi-elastic region ($v_i < v_c$), $\varepsilon$ was almost constant and ice spheres did not fracture at all. In the inelastic region ($v_i \geq v_c$), $\varepsilon$ decreased with increasing $v_i$ and ice spheres fractured. $\varepsilon$ was then fitted as $\varepsilon(v_i) = \varepsilon_{qe}(v_i/v_c)^{-\log(v_i/v_c)}$. The size dependencies of $\varepsilon$ in both regions were different. In the quasi-elastic region, the average value of $\varepsilon$ decreased with decreasing $r_p$ from $\varepsilon_{qe}$ = 0.95 ($r_p$ = 3.6 cm) to $\varepsilon_{qe}$ = 0.71 ($r_p$ = 0.14 cm). However, the maximum value of $\varepsilon$ in this region was close to unity and irrespective of $r_p$. In the inelastic region, $\varepsilon$ increased with decreasing $r_p$. $v_c$ was shown to increase with decreasing $r_p$ from 23 cm/s ($r_p$ = 3.6 cm) to 124 cm/s ($r_p$ = 0.14 cm). The size dependence of $v_c$ was explained by the strain-rate dependence of the fracture strength of ice.** 

*Key Words:* **restitution coefficient; ice; fracture strength; collision; planetary rings.**

## 1. INTRODUCTION

Saturn's rings consist mostly of water ice particles that range broadly in size from 1 cm to 5 m (Marouf *et al.* 1983, Cuzzi *et al.* 1984, Zebker *et al.* 1985) and that collide with each other in a rotating disk. The collision phenomena, including coagulation, rebound, and fragmentation, are important physical processes controlling the dynamics of ring particles (e.g., Greenberg *et al.* 1977, Goldreich and Tremaine 1978, Stewart *et al.* 1984, Ohtsuki 1992). Several experimental studies have been conducted on ice coagulation (Hatzes *et al.* 1991, Bridges *et al.* 1996, Supulver *et al.* 1997), rebound (Bridges *et al.* 1984, Hatzes *et al.* 1988, Dilley 1993, Supulver *et al.* 1995, Dilley and Crawford 1996, Higa *et al.* 1996), and fragmentation (Hartmann 1978).

[1] Present address: The Institute of Space and Astronautical Science, Kato Lab., 3-1-1, Yoshinodai Sagamihara Kanagawa 299, Japan.

The energy loss during rebound is characterized by the restitution coefficient ($\varepsilon$), which is defined as the ratio of the rebound velocity to the impact velocity, and which is an important parameter to calculate the orbital evolution of ring particles. To simulate the ring systems, the impact velocity, size, and temperature dependencies of $\varepsilon$ of ice spheres are required. The Santa Cruz group (e.g., Bridges *et al.* 1984, Hatzes *et al.* 1988, Supulver *et al.* 1995) has made measurements of $\varepsilon$ at low velocities ($\leq$2 cm/s) that are impact velocities in the present Saturn's rings. This group derived the impact velocity, size, and temperature dependencies of $\varepsilon$ at various surface conditions. According to Hatzes *et al.* (1988), the surface conditions of ice samples severely affect $\varepsilon$; in particular, frost-covered surfaces respond much less elastically than smooth surfaces.

Measurements of $\varepsilon$ have also been made at velocities higher than 2 cm/s in a previous study by the present authors (Higa *et al.* 1996; hereafter Paper I). In Paper I, we determined only the velocity and temperature dependencies of $\varepsilon$ in smooth frost-free ice spheres ($r_p$ = 1.5 cm). However, the size dependence of $\varepsilon$ is also required for a more fundamental understanding of the collisional properties of ice. In the present work, we measured $\varepsilon$ of smooth frost-free ice spheres of various sizes, and our results show that $\varepsilon$ is dependent on the sample size. Combining our present results with those of Paper I, we give an equation of $\varepsilon$ of the smooth frost-free ice spheres over a wide range of impact velocities, sizes, and temperatures.

## 2. EXPERIMENTAL METHODS

Smooth frost-free ice spheres of five different radii ($r_p$ = 0.14, 0.4, 0.8, 1.5, and 3.6 cm) were used for the experiments (Fig. 1). The smallest ice spheres ($r_p$ = 0.14 cm) were made by freezing distilled water droplets in liquid nitrogen using a method similar to that of Araoka and Maeno (1978) and an average eccentricity of 0.92 $\pm$ 0.04. The spheres were composed of pure polycrystalline ice of less than submillimeter radius. We selected non-crack samples for the experiment. The larger spheres were



0019-1035/98 $25.00

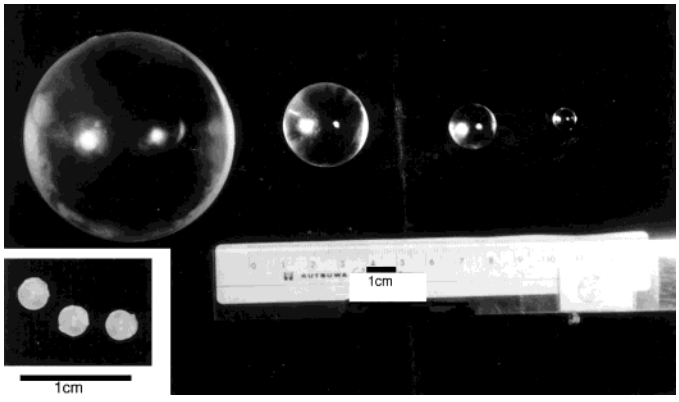


**FIG. 1.** A picture showing various ice spheres ($r_p$ = 0.14–3.6 cm).

formed by slowly melting an ice cube between a pair of brass molds at 15–25°C. The size of the target ice block was about $10 \times 10 \times 10$ cm$^3$ for the smaller spheres ($r_p$ = 0.14–1.5 cm) and $28 \times 28 \times 28$ cm$^3$ for the largest spheres ($r_p$ = 3.6 cm). The surface of the ice block was made as smooth as possible by planing and polishing. The larger spheres and blocks were made up of pure polycrystalline ice, which consisted of columnar grains of a few centimeters in radius. The mass ratios of the spheres to the blocks were smaller than 0.02, and thus we could approximate the collision as the impact on the semi-infinite target.

The impact experiments were carried out in a cold room at 261 ± 2.5 K, an ambient pressure of 1 bar, and relative humidity of 100%. Prepared samples were stored in this room under these conditions throughout the experiments. Head-on collisions were performed between an ice sphere and an ice block. Free falling was used to accelerate the ice sphere with a spring gun used only to obtain $v_i \geq 300$ cm/s for $r_p = 0.14$ cm.

The restitution coefficient of the ice sphere was defined as the ratio of the rebound velocity ($v_r$) to the impact velocity ($v_i$):

$$\varepsilon = \frac{v_r}{v_i}. \tag{1}$$

The velocities of the ice sphere were measured by either high-speed video camera (200 or 500 frames/s) or acoustic emission (AE) signals. The latter method was similar to that used by Yen *et al.* (1970) and enabled us to calculate velocities accurately from time intervals between bounces. The AE-sensor attached to the ice block surface detected precise collision times, and signals were monitored by a digital oscilloscope. The impact velocity of the $j$th bounce ($v_{i,j}$), where $j$ is the number of the bounce, was calculated from the time interval between the $(j-1)$th and $j$th bounces ($\Delta t_j$, $j \geq 2$), $v_{i,j} = g\,\Delta t_j/2$, where $g$ is gravity acceleration. The initial velocity ($v_{i,1}$) was calculated from the known height of the free fall ($h$), $v_{i,1} = \sqrt{2gh}$. Similarly, the rebound velocity of the $j$th bounce ($v_{r,j}$) was calculated as $v_{r,j} = g\,\Delta t_{j+1}/2$. When fracturing occurred at the first bounce, $v_{r,1}$ was measured for the largest fragment and subsequent $\varepsilon$ data of $j > 2$ were not used.

In our AE method, a problem that a systematic error in low velocity measurements for $v_i <$ about 5 cm/s to obtain $v_i$, $v_r$, and $\varepsilon$ occurs when the height of the bounce is comparable to the surface roughness (for an example, the vertical height of the bounce is of order 100 $\mu$m at 5 cm/s). This error increases as velocities decrease, although the appearance of a sample surface looks very smooth and frost-free as a result of careful preparation of samples. We cannot deny that our data include uncertainties due to such surface roughness. However, this error is small for $v_i >$ about 5 cm/s.

## 3. RESULTS

The collisional behavior of ice spheres was classified into three types as in Paper I: no-crack type (NC), crack type (C), and fragmentation type (F). In the NC type, no visible cracks or plastic deformations were observed at the impact points of either the ice sphere or block. However, tiny white marks were sometimes visible at higher impact velocities of the NC type and were probably similar to those observed by the experiments of the Santa Cruz group. In the C type, many tiny cracks (white region in Fig. 2a), were formed around the impact point, and small fragments were formed. With the increase of $v_i$, vertical cracks were observed to grow from the impact point. In the F type, the vertical cracks grew and broke the sphere into a few pieces (Fig. 2b). The C and F types were distinguished by the ratio of the largest fragment mass to the initial mass of the ice sphere ($m_l/m_p$): for the C type, $0.95 \leq m_l/m_p \leq 1$, and for the F type, $m_l/m_p < 0.95$.

Figure 3 shows the deformation types observed at various radii and impact velocities. The result of $r_p = 0.14$ cm was shown by only the NC and C types, because the generated fragments were too small to observe, and thus it was impossible to distinguish the C from the F types. The samples collected after collision showed that the degree of fracture of both ice spheres and blocks increased with increasing $v_i$, and also increased with increasing $r_p$. The normalized largest fragment mass rapidly decreased with increasing $v_i$. It is noteworthy that the onset velocity of fracturing increased with decreasing $r_p$.

Figures 4a–4e show $\varepsilon$ as a function of $v_i$ for various $r_p$ at 261 K. The velocity dependence can be classified into a quasi-elastic region ($v_i < v_c$) and an inelastic region ($v_i \geq v_c$), as discussed in Paper I. In the quasi-elastic region, $\varepsilon$ is almost constant and corresponds to the NC type region. We call this region "quasi-elastic" because $\varepsilon$ is not exactly

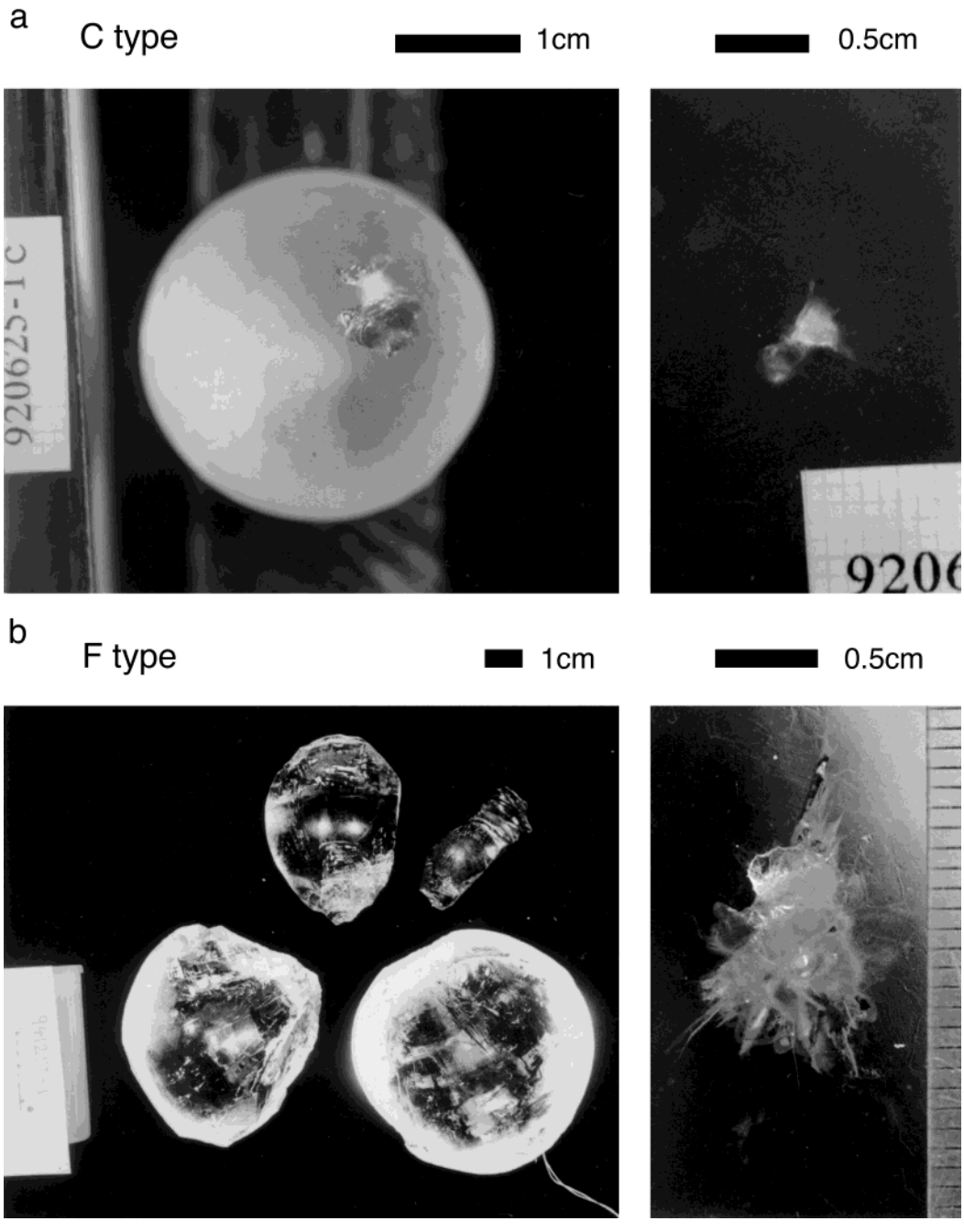


**FIG. 2.** Photographs of ice spheres (left) and ice block surfaces (right). (a) C type ($m_l/m_p = 0.99$, $r_p = 1.5$ cm, $T = 245$ K, $v_i = 150$ cm/s, $\varepsilon = 0.80$). (b) F type ($m_l/m_p = 0.51$, $r_p = 3.6$ cm, $T = 261$ K, $v_i = 436$ cm/s, $\varepsilon = 0$).

unity; i.e., the behavior is not purely elastic. In the inelastic region, $\varepsilon$ decreases with increasing $v_i$ and corresponds to the region of the C and F types, meaning that the decrease of $\varepsilon$ is related to fracturing.

To obtain an empirical equation of $\varepsilon$ for various $r_p$, we calculated the average values for the NC type as the typical values in the quasi-elastic region ($\varepsilon_{qe}$) and used the following empirical equation with $\varepsilon_{qe}$ to fit $\varepsilon$ in the inelastic region,

$$\varepsilon = \varepsilon_{qe}\left(\frac{v_i}{v_c}\right)^{-\log(v_i/v_c)} \qquad v_i \geq v_c, \tag{2}$$

where $v_c$ is the critical velocity. Equation (2) is different

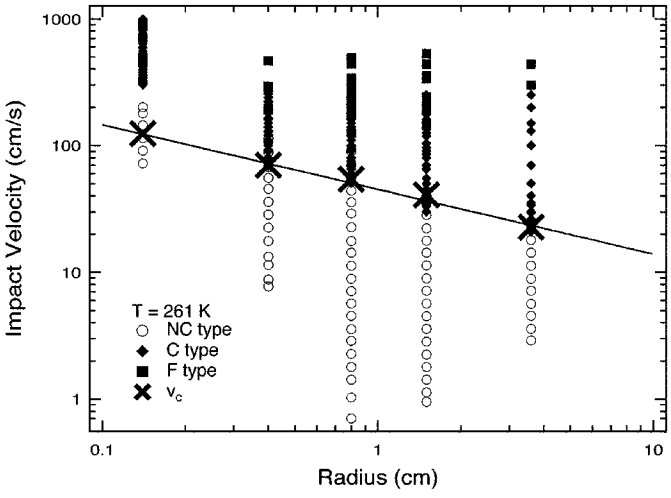


**FIG. 3.** Diagram showing the collision type for various $r_p$ at 261 K. The line indicates relation between $v_c$ and $r_p$, which separates the quasi-elastic and inelastic regions. This line corresponds to the onset of fracturing.

from the equation $\varepsilon = (v_i/v_c)^{-\log(v_i/v_c)}$ in Paper I, because the former provides a better fit to the data. Equation (2) shows that $\varepsilon$ approaches $\varepsilon_{qe}$ as $v_i$ goes to $v_c$. A least-squares fit of Eq. (2) was applied to the C type data. Table I summarizes the $\varepsilon_{qe}$ and $v_c$ resulting from the present data and the refined data in Paper I.

The obtained $\varepsilon_{qe}$ decreased from 0.95 ± 0.04 ($r_p$ = 3.6 cm) to 0.71 ± 0.09 ($r_p$ = 0.14 cm) with decreasing $r_p$. On the other hand, as shown in Figs. 4a–4e, the highest values of $\varepsilon$ in the quasi-elastic region were close to unity and independent of $r_p$. Additionally, the data were more scattered at smaller $r_p$. The values of $v_c$ increased from 23 cm/s ($r_p$ = 3.6 cm) to 124 cm/s ($r_p$ = 0.14 cm) with decreasing $r_p$. It is notable that $v_c$, which divides the quasi-elastic region from the inelastic region, coincided with the onset velocity of fracturing, as shown in Fig. 4. However, in the case of $r_p$ = 0.14 cm, since the formed cracks were too small to be observed around the transition velocity from the NC type to the C type, the boundary of deformation types was rather ambiguous.

## 4. DISCUSSION

### *4.1. Restitution Coefficients in the Quasi-elastic Region*

We here attempt to describe the impact velocity and size dependencies of $\varepsilon_{qe}$ as a typical value in the quasi-elastic region using a viscous dissipation model (Dilley 1993). Dilley (1993) proposed the viscous dissipation model for $\varepsilon$ of ice spheres with a frosted surface to explain the velocity and size dependencies of $\varepsilon$ under frosted-surface conditions. For the collision between two ice spheres of radius $r_p$ (mass $m_p$) and $r_t$ (mass $m_t$), Dilley describes $\varepsilon$ as

$$\varepsilon = \exp(-\pi\xi/\sqrt{1-\xi^2}), \tag{3}$$

where

$$\xi = \xi_0(1+\gamma^3)^K(1+\gamma)^{0.2}\left(\frac{r_p}{2.5\text{ cm}}\right)^{-3K-0.2} v_i^{p}, \tag{4}$$

and

$$\gamma = r_p/r_t \le 1. \tag{5}$$

The constants $\xi_0$, $p$, and $K$ are determined empirically using experimental data. This model could describe the frosted-surface ice data of both Hatzes *et al.* (1988) and Dilley and Crawford (1996). The derived constants are thus $\xi_0$ = 0.16, $p$ = 0.65, and $K$ = 0.6.

When this model is applied to $\varepsilon_{qe}$, the visco-elastic property of the frost-free surface of our sample can be obtained. Because $\varepsilon_{qe}$ is irrespective of $v_i$, $p$ is zero. Inserting $\varepsilon_{qe}$ into Eq. (3), we obtain $\xi$ at various $r_p$ (Fig. 5). Using Eq. (4) and $\gamma$ = 0, the calculated $\xi$ was fitted as

$$\xi = 0.027\left(\frac{r_p}{2.5\text{ cm}}\right)^{-0.5}. \tag{6}$$

Therefore, the general equation for arbitrary sizes is

$$\xi = 0.027(1+\gamma^3)^{0.1}(1+\gamma)^{0.2}\left(\frac{r_p}{2.5\text{ cm}}\right)^{-0.5}. \tag{7}$$

Figure 6 shows the size dependence of $\varepsilon_{qe}$ for $\gamma$ = 0 and $\gamma$ = 1. The size dependence of $\varepsilon_{qe}$ is well described by Dilley's model. The obtained constants are different from those determined using the data of either Hatzes *et al.* (1988) or Dilley and Crawford (1996). These differences are due to the surface conditions (irregular, frosted, or rough surfaces, surface layer thickness, etc.).

In Dilley's model, it was assumed that the restitution behavior was expressed by a vibration of the Kelvin–Voigt body and that the energy loss was caused in a surface layer of frost through viscous dissipation. Therefore, the viscosity was proportional to $v_i^p$, and the period of vibration was proportional to $M^{-K}$, where $M$ is the reduced mass defined by Eq. (A-4) and $M \propto r_p^3/(1+\gamma^3)$. Our result, $p$ = 0, indicates that the viscosity of the ice surface is a constant. Thus the surface behaves as a Newtonian fluid. Our smaller value of $K$ = 0.1 indicates that the mass effect is smaller than that estimated by Dilley and Crawford (1996).

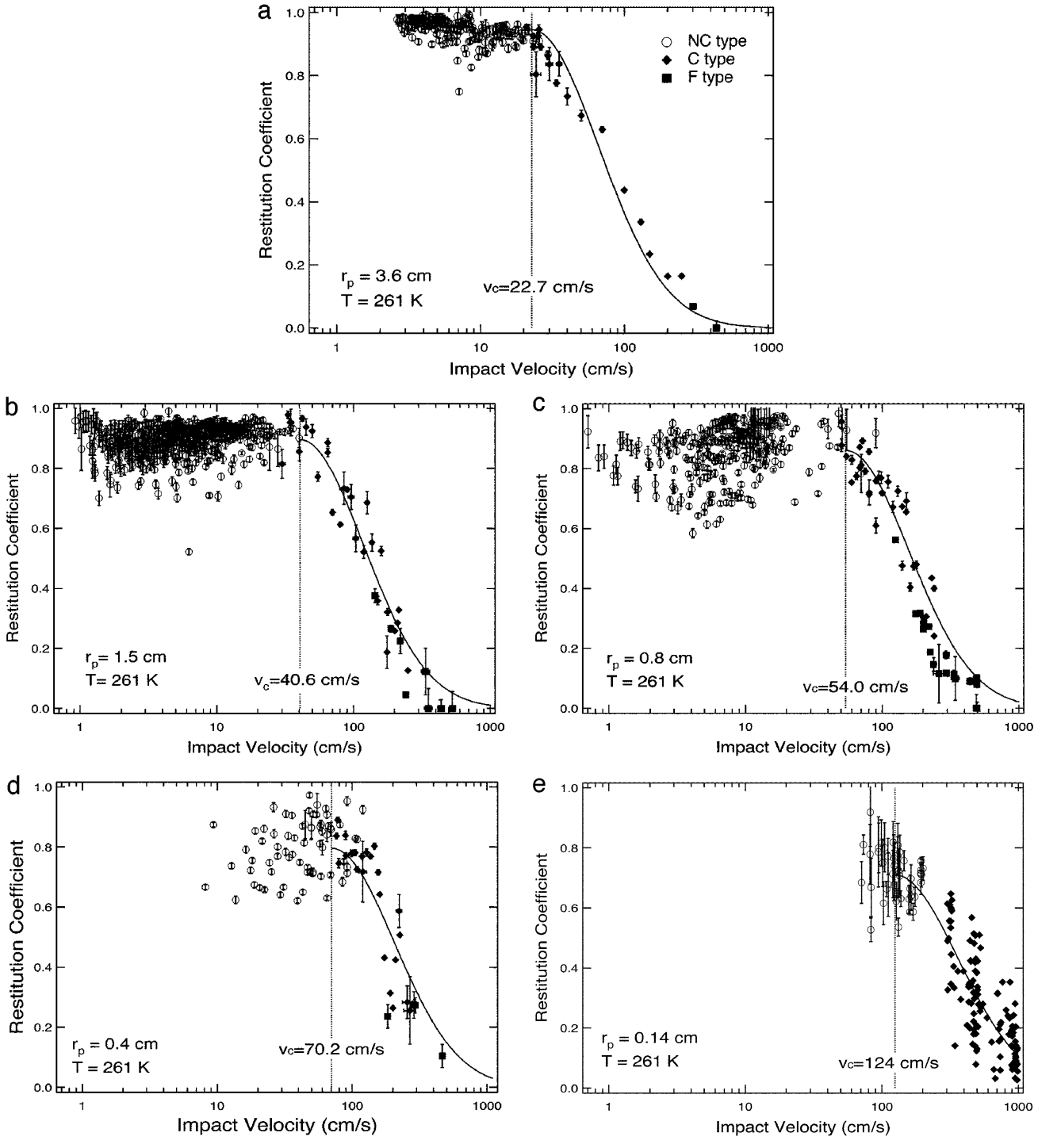


**FIG. 4.** Restitution coefficient as a function of $v_i$ for various $r_p$ at 261 K. (a) $r_p$ = 3.6 cm, (b) $r_p$ = 1.5 cm, (c) $r_p$ = 0.8 cm, (d) $r_p$ = 0.4 cm, (e) $r_p$ = 0.14 cm.

### *4.2. Restitution Coefficients in the Inelastic Region*

We attempt to explain the impact velocity and size dependencies of $\varepsilon$ in the in-elastic region by classical plastic deformation models such as Andrews' model (Andrews 1930; see also Borderies *et al.* 1984 and Dilley 1993) and Johnson's model (Johnson 1985). In both models, the amount of energy dissipation is proportional to the yielding volume and the yield stress, which are calculated by the stress distribution derived from the elastic impact theory

**TABLE I**
**Experimental Results of the Average Value ($\varepsilon_{qe}$) and the Critical Velocity ($v_c$)**

| Radius (cm) | Temperature (K) | $\varepsilon_{qe}$ | $v_c$ (cm/s) | Surface condition | Note |
|---|---|---|---|---|---|
| 3.6 | 261 ± 1.3 | 0.95 ± 0.04 | 22.7 | Frost-free | |
| 1.5 | 261 ± 2.0 | 0.89 ± 0.05 | 40.6 | Frost-free | Paper I[a] |
| 0.8 | 261 ± 2.1 | 0.86 ± 0.09 | 54.0 | Frost-free | |
| 0.4 | 261 ± 2.1 | 0.79 ± 0.09 | 70.2 | Frost-free | |
| 0.14 | 261 ± 2.1 | 0.71 ± 0.09 | 124 | Frost-free | |
| 1.5 | 269 ± 1.8 | 0.89 ± 0.05 | 29.2 | Frost-free | Paper I[a] |
| 1.5 | 245 ± 2.2 | 0.86 ± 0.08 | 77.6 | Frost-free | Paper I[a] |
| 1.5 | 215 − 113 ±2.5 | 0.87 ± 0.03[b] | 180[c] | Frosty | Paper I[a] |

[a] Data from Paper I.
[b] The maximum value in NC types.
[c] The $v_c$ was estimated from the velocity of the onset of ice fracturing.

(the Hertz theory) in the Appendix. Both models predict that $\varepsilon$ for $v_i < v_{pd}$ is unity and that $\varepsilon$ for $v_i \geq v_{pd}$ is described as a function of $v_i$ having only the single parameter $v_{pd}$, where $v_{pd}$ is the velocity at the onset of yielding.

Because ice is a visco-elastic material, fracturing is necessarily accompanied by plastic deformation. It follows, then, that $v_c$ (the velocity at the onset of fracturing) is the upper limit of $v_{pd}$ (the velocity at the onset of yielding). However, the velocity dependencies of $\varepsilon$ calculated by the two models were in poor agreement with our results. Therefore, in order to explain the velocity dependence of $\varepsilon$ in the inelastic region, we need a new model that includes the crack formation.

Moreover, according to the plastic deformation models, the parameter $v_{pd}$ of both models is proportional to $\sqrt{R^3/M}$, where $M$ and $R$ are the reduced mass and radius defined by Eqs. (A-4) and (A-5). Our experimental conditions give $M \simeq m_p$ and $R \simeq r_p$, and then the size dependence of $v_{pd}$ is canceled. However, our results clearly show the size dependence of $v_c$. This size dependence must be closely related to fracturing of ice in collision, and we will make a theoretical consideration of the fracture strength of ice in collision.

### 4.3. Size Dependence of the Critical Velocity

*4.3.1. Fracture strength of ice in collision.* In order to analyze the size dependence of $v_c$, let us consider the head-on collision of two spherical elastic bodies. Figure 7 shows the deformation of spheres of radius $r_p$ (mass $m_p$) and $r_t$ (mass $m_t$) at the maximum compression strain state, where we choose a cylindrical coordination system ($r$, $\theta$, $z$) and take the line between centers of the two spheres as the $z$-

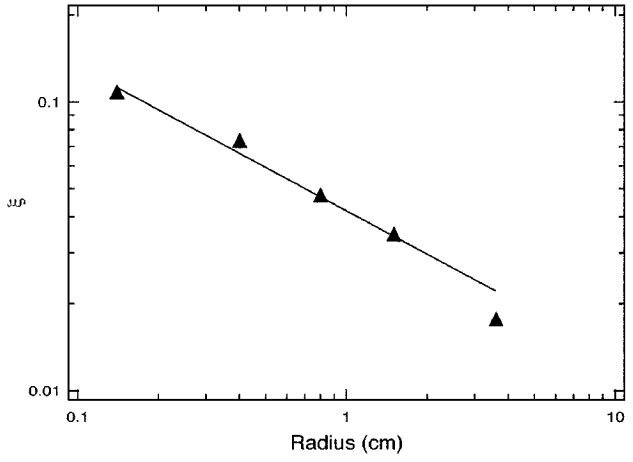


**FIG. 5.** Relation between Dilley's parameter $\xi$ and $r_p$ at 261 K.

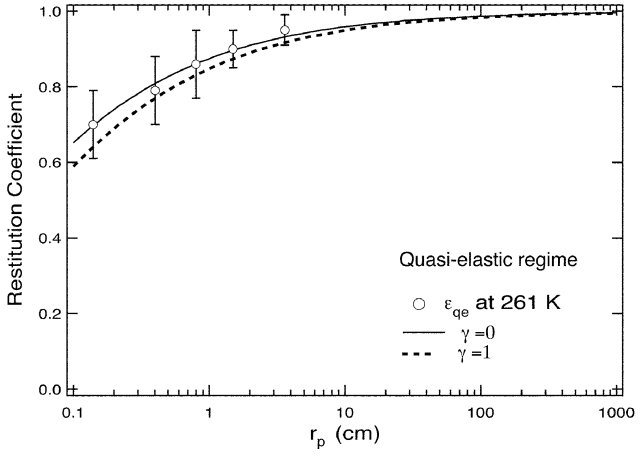


**FIG. 6.** The average values, $\varepsilon_{qe}$, predicted by Dilley's model. The solid and broken curves indicate collisions at $\gamma = 0$ and $\gamma = 1$, respectively. Our results of $\varepsilon_{qe}$ at 261 K are also plotted.

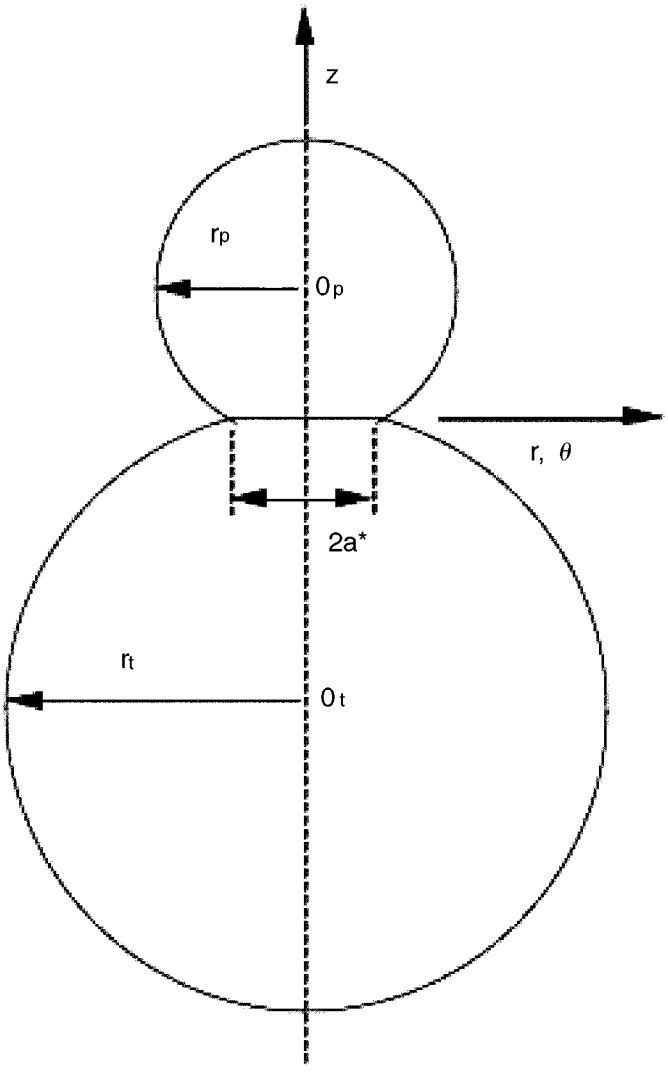


**FIG. 7.** Schematic picture of elastic contact at the maximum strain state.

axis ($O_pO_t$) and $r - \theta$ plane normal to the $z$-axis. Then the stress and strain in collision can be calculated using the elastic impact theory. When the impact velocity is $v_i$, the maximum radius of the area of contact ($a^*$), the maximum pressure ($p_0^*$), and the time of maximum compression ($t^*$) are given by the analytical formulations Eqs. (A-1), (A-2), and (A-3), respectively. This theory is based on the assumption that the deformation can be treated as quasi-static in the collisions. Johnson (1985) states that the quasi-static approximation is valid for the condition of $0.4\, Rv_i/a^*C_0 \ll 1$ (or $0.3(v_i/C_0)^{3/5} \ll 1$ for two like sphere collision), where $C_0$ is the bulk sound velocity. The criterion for the quasi-static approximation in the present experiments is less than approximately $10^{-2}$ ($v_i < 10^3$ cm/s, $C_0 \simeq 3 \times 10^5$ cm/s), and therefore we can apply the elastic impact theory.

By calculating the stress distribution within the contact area at the maximum compression strain state (Johnson 1985; see also Huber 1904, Morton and Close 1922, Timoshenko and Goodier 1951), the maximum shear stress ($\tau^*_{max}$) is found to occur directly beneath the impact point along the $z$-axis and is given by

$$\tau^*_{max} = \max.\{|\sigma^*_z - \sigma^*_{r,\theta}|/2\},$$

where $\sigma^*_z$, $\sigma^*_r$, and $\sigma^*_\theta$ are the principal stresses along the $z$-axis,

$$\frac{\sigma^*_z}{p^*_0} = -(1 + z^2/a^{*2})^{-1}, \tag{8}$$

$$\frac{\sigma^*_r}{p^*_0} = \frac{\sigma^*_\theta}{p^*_0} = -(1 + \nu)\{1 - (z/a^*)\arctan(a^*/z)\} + \frac{1}{2}(1 + z^2/a^{*2})^{-1}. \tag{9}$$

We use the material properties of ice, the density 920 kg/m$^3$, Poisson's ratio $\nu = 0.31$ (Gold 1958), Young's modulus $E$ given by Dantl (1968) (see also Hobbs 1974). In the case of an ice-on-ice impact, $\tau^*_{max}$ is given by

$$\tau^*_{max} = 0.31 p^*_0 \tag{10}$$

at depth of $z = 0.48a^*$. On the other hand, the maximum tensile stress occurs at the very edge of contact ($r = a^*$) and is given by $(1 - 2\nu)p^*_0/3$. Two crack types will theoretically occur according to the stress fields. The maximum shear stress makes shear cracks in the contact area of impact samples. The maximum tensile stress makes tensile cracks on the circular edge of the contact area.

When we consider the criterion of the fracture strength in collision, it is necessary to know which stress initiates the fracture in the experiments. The ratio of the maximum shear stress to the maximum tensile stress derived from the elastic impact theory is about 2.4. According to the uniaxial deformation tests of Hawkes and Mellor (1972), the compressive and tensile strengths of ice at temperature 266 K and strain rate $9.86 \times 10^{-3}$ s$^{-1}$ were 6.68–9.18 MPa and 2.06–2.18 MPa, respectively. The ratio of the shear strength to the tensile strength can then be calculated as 1.5–2.4, a value almost equal to that derived from the elastic impact theory. This means that the maximum shear stress overcomes the shear strength when the maximum tensile stress overcomes the tensile strength. From our observations, the onset of the shear crack and tensile crack occurred at the same time. Since this observation is consistent with the above theoretical consideration, we choose

the shear stress as the criterion for the fracture strength in collision for convenience.

According to Eq. (A-2), the relation among $\tau^*_{max}$, $v_i$, $M$, and $R$ is given by

$$\tau^*_{max} \propto p^*_0 \propto M^{1/5} R^{-3/5} v_i^{2/5}. \quad (11)$$

In the case of a like-material collision between spheres, this equation becomes

$$\tau^*_{max} \propto (1+\gamma^3)^{-1/5}(1+\gamma)^{3/5} v_i^{2/5}, \quad (12)$$

where $\gamma = r_p/r_t$. The shear fracture occurs when $\tau^*_{max}$ overcomes the fracture strength. Therefore, $\tau^*_{max}$ at $v_c$ is the fracture strength of ice ($\tau^*_s$). Substitution of $v_i = v_c$ and $\tau^*_{max} = \tau^*_s$ in Eqs. (11) and (12) leads to

$$v_c \propto \tau_s^{*5/2}\sqrt{R^3/M} \propto \tau_s^{*5/2}(1+\gamma^3)^{1/2}(1+\gamma)^{-3/2}. \quad (13)$$

Since $\gamma = 0$ in our experimental condition, the size dependence of $v_c$ vanishes. However, our data show the clear size dependence of $v_c$. This result indicates that the fracture strength of ice depends on the radius. One of the possible explanations for this dependence is that there exists a size dependence of the material strength. The fact that larger samples are likely to contain larger flaws leads to the size dependence of the material strength. According to the Griffith model, the flaws control the material strength, and thus the strength is proportional to the inverse square root of size. However, present results show $\tau^*_s \propto r_p^{-1/5}$, so that the size dependence of $\tau^*_s$ cannot be adequately explained by the intrinsic flaws described by the Griffith model.

*4.3.2. Strain rate at the onset of fracturing.* Another possible explanation for the size dependence of $v_c$ is that there exists a strain-rate dependence of the material strength. The strength of ice depends on strain rates and temperatures. According to the uniaxial compression tests ($T$ = 100–263 K; strain rate = $4 \times 10^{-3}$–$4 \times 10^{-6}$ s$^{-1}$) of Arakawa and Maeno (1997), the strength of ice became greater with increasing strain rates and decreasing temperatures and the yield stress in the ductile region and the fracture stress in the brittle region were expressed by the similar relation

$$\dot{\varepsilon} = A\sigma^n \exp\left(-\frac{Q}{RT}\right), \quad (14)$$

where $\dot{\varepsilon}$ is the strain rate, $\sigma$ the stress, $Q$ the activation energy, $R$ the gas constant, $T$ the temperature, and $A$ and $n$ constants (see also Arakawa and Maeno 1992, Arakawa 1995). It is convenient that the static and dynamic fracture strengths are described by the same relationship as in Eq. (14). We can therefore estimate the strain rate in the collision as a function of size and velocity and discuss a relation between the fracture strength and the strain rate.

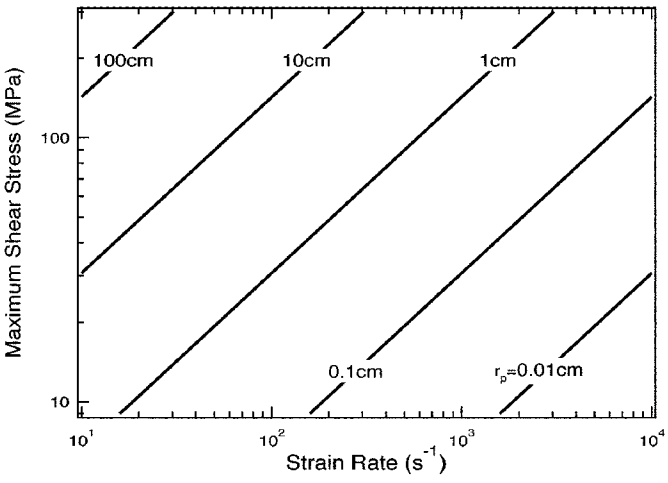


**FIG. 8.** Relation between $\tau^*_{max}$ and $\dot{\varepsilon}^*_z$ at 261 K and $\gamma = 0$.

From Hooke's law, the strain along the $z$-axis at the maximum shear stress point is given by

$$\varepsilon^*_z = \frac{1}{E}\sigma^*_z - \frac{\nu}{E}\sigma^*_r - \frac{\nu}{E}\sigma^*_\theta, \quad (15)$$

where $\sigma^*_z$, $\sigma^*_r$, and $\sigma^*_\theta$ are defined by Eqs. (8) and (9). This strain is achieved at the time of maximum compression $t^*$ so that the strain rate can be estimated as

$$\dot{\varepsilon}^*_z \simeq \frac{\varepsilon^*_z}{t^*}. \quad (16)$$

In the case of an ice-on-ice impact, $\dot{\varepsilon}^*_z$ is given by

$$\dot{\varepsilon}^*_z = \frac{0.69 p^*_0}{Et^*} \quad (17)$$

at the depth of $z = 0.48a^*$.

According to Eqs. (A-2) and (A-3), the relation among $\dot{\varepsilon}^*_z$, $v_i$, $M$, and $R$ is given by

$$\dot{\varepsilon}^*_z \propto p^*_0/t^* \propto M^{-1/5} R^{-2/5} v_i^{3/5}. \quad (18)$$

In the case of a like-material collision, this equation becomes

$$\dot{\varepsilon}^*_z \propto (1+\gamma^3)^{1/5}(1+\gamma)^{2/5} r_p^{-1} v_i^{3/5}. \quad (19)$$

It is noted that $\dot{\varepsilon}^*_z$ increases with decreasing $r_p$ but $\tau^*_{max}$ is independent of $r_p$ as given by Eq. (12), when $\gamma$ and temperature are constants. Therefore, the $\tau^*_{max}$ vs $\dot{\varepsilon}^*_z$ curves for various $r_p$ and $v_i$ show different paths as shown in Fig. 8. This is the reason for the size dependence of $v_c$.

**TABLE II**
**Calculated Results of the Fracture Strength ($\tau_s^*$) and the Strain Rate ($\dot{\varepsilon}_s^*$)**

| Radius (cm) | Temperature (K) | $v_c$ (cm/s) | $\tau_s^*$ (MPa) | $\dot{\varepsilon}_s^*$ ($s^{-1}$) |
|---|---|---|---|---|
| 3.6 | 261 | 22.7 | 34.0 | $3.23 \times 10^1$ |
| 1.5 | 261 | 40.6 | 42.9 | $1.10 \times 10^2$ |
| 0.8 | 261 | 54.0 | 48.0 | $2.44 \times 10^2$ |
| 0.4 | 261 | 70.2 | 53.4 | $5.72 \times 10^2$ |
| 0.14 | 261 | 124 | 67.0 | $2.30 \times 10^3$ |
| 1.5 | 269 | 29.2 | 37.3 | $8.99 \times 10^1$ |
| 1.5 | 245 | 77.6 | 56.3 | $1.63 \times 10^2$ |
| 1.5 | 213 | 180 | 80.7 | $2.71 \times 10^2$ |
| 1.5 | 193 | 180 | 81.8 | $2.72 \times 10^2$ |
| 1.5 | 173 | 180 | 82.9 | $2.73 \times 10^2$ |
| 1.5 | 153 | 180 | 83.9 | $2.74 \times 10^2$ |
| 1.5 | 123 | 180 | 85.1 | $2.75 \times 10^2$ |
| 1.5 | 113 | 180 | 85.2 | $2.75 \times 10^2$ |

*Note.* When we calculate $\tau_s^*$ and $\dot{\varepsilon}_s^*$ we use the density 920 kg/m$^3$, Poisson's ratio $\nu = 0.31$ (Gold 1985), and Young's modulus $E = 1/(10.40(1 + 1.070 \times 10^{-3}\, T + 1.87 \times 10^{-6}\, T^3))$ in units of $10^2$ GPa and °C (Dantl 1968; see also Hobbs 1974).

Substituting $v_i = v_c$ into Eqs. (10) and (17), we get the fracture strength $\tau_s^*$ and the strain rate $\dot{\varepsilon}_s^*$ generated at $v_c$. The calculated $\tau_s^*$ and $\dot{\varepsilon}_s^*$ are given in Table II. The relationship between $\tau_s^*$ and $\dot{\varepsilon}_s^*$ at 261 K, shown in Fig. 9, is well described by the power law equation

$$\tau_s^* = A_s \dot{\varepsilon}_s^{*1/n_s}, \tag{20}$$

where $n_s$ and $A_s$ are constants. By means of the least-squares method, $A_s$ is estimated as 20 (MPa $s^{n_s}$) and $n_s$ as 6.5. The value, $n_s = 6.5$, agrees with $n = 5.8$–$7.1$ of the brittle region that obtained by Arakawa and Maeno (1997). The strain-rate dependence of $\tau_s^*$ is well described by the equation similar to Eq. (14). The size dependence of $v_c$ could be explained by the fact that the fracture strength of ice varied with the strain rate: $\dot{\varepsilon}_s^*$ increases with decreasing $r_p$ so that $\tau_s^*$ increases, and, on the other hand, $\dot{\varepsilon}_s^*$ decreases with increasing $r_p$ so that $\tau_s^*$ decreases.

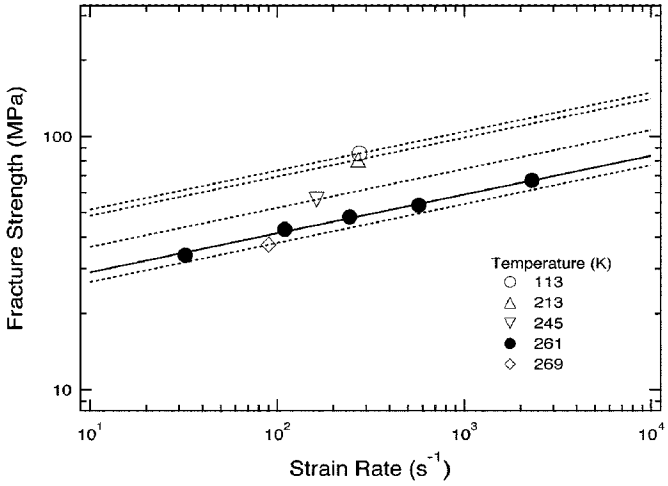


**FIG. 9.** Relation between $\tau_s^*$ and $\dot{\varepsilon}_s^*$ at 269–113 K.

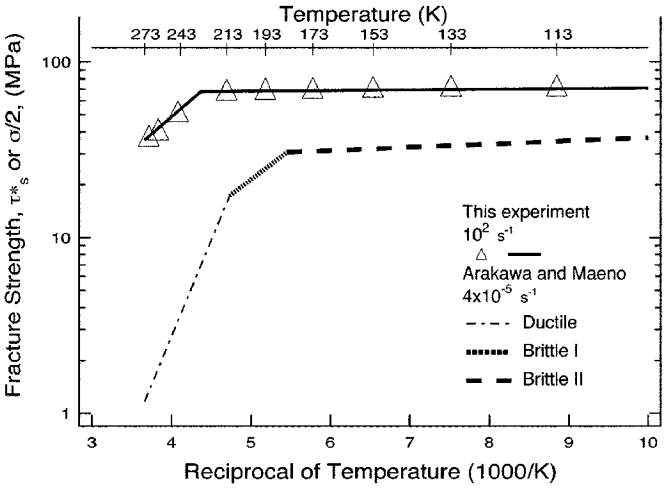


**FIG. 10.** Relation between the estimated fracture strength and the reciprocal of temperature at $\dot{\varepsilon}_s^* = 10^2$ $s^{-1}$. The results of Arakawa and Maeno (1997) at strain rate $4 \times 10^{-5}$ $s^{-1}$ are also plotted.

*4.3.3. Empirical relations of fracture strength in collision.* Finally, we extend Eq. (20) to an equation that includes the temperature. Figure 9 plots $\tau_s^*$ against $\dot{\varepsilon}_s^*$ given by the refined results of Paper I. $\tau_s^*$ clearly increased with the decreasing $T$. If we assume that $n_s$ is irrespective of $T$ and that the temperature dependence of $\tau_s^*$ are described by equation similar to Eq. (14), we can write the temperature dependence as

$$\dot{\varepsilon}_s^* = A_s' \tau_s^{*n_s} \exp\left(-\frac{Q_s}{RT}\right), \tag{21}$$

where $A_s'$ is a constant and $Q_s$ is the activation energy related to the crack formation. Using this equation, we can estimate $\tau_s^*$ at any temperature. The estimated relations between $\tau_s^*$ and $\dot{\varepsilon}_s^*$ at various $T$ are shown as broken lines in Fig. 9. For example, $\tau_s^*$ at $\dot{\varepsilon}_s^* = 10^2$ $s^{-1}$ against the reciprocal of temperature is shown in Fig. 10. The temperature dependence changes at 229 K. At temperatures higher than 229 K, $\tau_s^*$ increases with decreasing temperature. By means of the least-squares method, $Q_s$ is estimated as 48.2 kJ/mol. At temperatures lower than 229 K, $\tau_s^*$ is almost constant.

In Fig. 10, we compare our result with that of Arakawa and Maeno (1997). The Ductile and Brittle I and II indicate

ductile deformation and brittle fracture, respectively. Similar temperature dependencies are seen when ice fractured in a brittle manner. The higher temperature region ($T \geq 229$ K) corresponds to Brittle I, and the obtained value, $Q_s = 48.2$ kJ/mol ($T \geq 229$ K), is in accordance with $Q = 37$–$62$ kJ/mol of Brittle I. The lower temperature region ($T < 229$ K) corresponds to Brittle II.

## 5. CONCLUSIONS AND IMPLICATION TO SATURN'S RINGS

We find that the size and temperature dependencies of $v_c$ are explained by the strain-rate and temperature dependencies of the fracture strength of ice. Using the relation given by Eqs. (12) and (19) and neglecting the temperature dependence of Young's modulus $E$, Eq. (21) is expressed by an equation of $v_c$ as a function of $\gamma$, $r_p$, and $T$,

$$v_c \simeq v_0(1+\gamma^3)^a(1+\gamma)^b r_p^c \exp\left(-c\frac{Q_s}{RT}\right), \qquad (22)$$

and

$$a = \frac{n_s+1}{2n_s-3}, \qquad b = -\frac{3n_s-2}{2n_s-3}, \qquad c = -\frac{5}{2n_s-3}, \qquad (23)$$

where $v_0$, $n_s$, and $Q_s$ are constants and determined empirically using experimental data. Ultimately, we get the equations:

$$v_c = \begin{cases} 5.72\times10^{-4}\exp\left(\dfrac{48.2\times10^3}{2RT}\right) & \\ \qquad \times(1+\gamma^3)^{3/4}(1+\gamma)^{-7/4}\left(\dfrac{r_p}{1.5\text{ cm}}\right)^{-1/2} & T \geq 229\text{ K}, \\ 180(1+\gamma^3)^{3/4}(1+\gamma)^{-7/4}\left(\dfrac{r_p}{1.5\text{ cm}}\right)^{-1/2} & T < 229\text{ K}. \end{cases} \qquad (24)$$

Thus we can extrapolate our result to arbitrary size collisions at various $T$. The resultant size and temperature dependencies of $v_c$ are shown in Fig. 11.

On the basis of the above result, $\varepsilon$ of smooth and frost-free ice at the Saturn's temperature condition $\simeq$100 K can be described as

$$\varepsilon = \begin{cases} \sim 1 & v_i < v_c, \\ \left(\dfrac{v_i}{v_c}\right)^{-\log v_i/v_c} & v_i \geq v_c, \end{cases} \qquad (25)$$

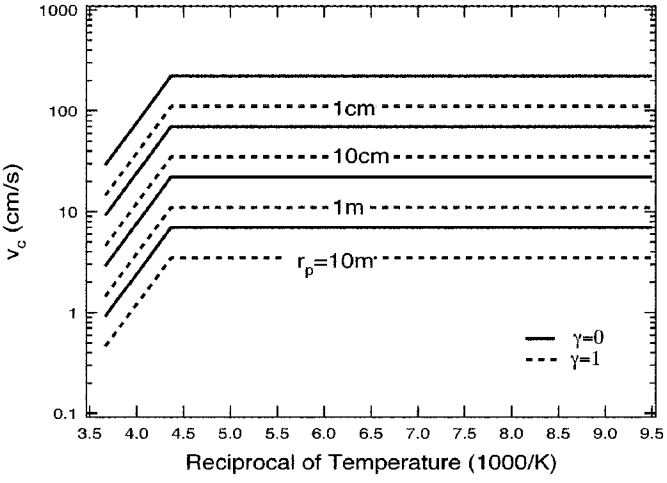


**FIG. 11.** Size and temperature dependencies of $v_c$.

where $v_c$ is given by Eq. (24). When the ring particles are smooth frost-free ice spheres, calculations of the orbital evolution can be made using the above results. The present results show that $\varepsilon$ of ring particles ranging from 1 cm to 5 m is unity at collision velocities up to 5 cm/s ($r_p = 5$ m) and 100 cm/s ($r_p = 1$ cm). These elastic values are too high to explain the present Saturn ring system. Thus, it is unlikely that smooth and frost-free surfaces are present in the ring system now.

Even if the particle surfaces were initially smooth and frost-free, they might undergo cracking and fracturing at higher impact velocities due to the increasing velocity dispersion. Although there are other erosion effects (e.g., ion sputtering, photosputtering and micrometeoroids), their surfaces would be rapidly eroded and covered with a layer of ejected ice fragments as an inevitable consequence of collisions. Thus, $\varepsilon$ of ring particles decreases rapidly.

## APPENDIX: ELASTIC DEFORMATION OF COLLIDING SPHERES: THE HERTZ THEORY

Let us consider the collision of two spherical elastic bodies. The strain and stress are obtained using the elastic impact theory, e.g., Johnson (1985). When two spheres of radius $r_p$ (mass $m_p$) and $r_t$ (mass $m_t$) collide with a relative velocity $v_i$ along their line of centers, the maximum radius of the area of contact $a^*$ and the maximum value of pressure $p_0^*$ during collision are given by

$$a^* = \left(\frac{15}{16}\right)^{1/5} E^{*-1/5} M^{1/5} R^{2/5} v_i^{2/5}, \qquad (A\text{-}1)$$

$$p_0^* = \frac{3}{2\pi}\left(\frac{4}{3}\right)^{4/5}\left(\frac{5}{4}\right)^{1/5} E^{*4/5} M^{1/5} R^{-3/5} v_i^{2/5}. \qquad (A\text{-}2)$$

The time of maximum compression $t^*$ is given by

$$t^* = 1.435 E^{*-2/5} M^{2/5} R^{-1/5} v_i^{-1/5}, \qquad (A\text{-}3)$$

where $M$ and $R$ are the reduced mass and radius,

$$\frac{1}{M} = \frac{1}{m_p} + \frac{1}{m_t}, \tag{A-4}$$

$$\frac{1}{R} = \frac{1}{r_p} + \frac{1}{r_t}, \tag{A-5}$$

and $E^*$ is defined as

$$\frac{1}{E^*} = \frac{1 - \nu_p^2}{E_p} + \frac{1 - \nu_t^2}{E_t}, \tag{A-6}$$

and $E$ = Young's modulus, $\nu$ = Poisson's ratio, and the suffixes $p$ and $t$ correspond to projectile and target, respectively.

## ACKNOWLEDGMENTS

The authors acknowledge Dr. K. Ohtsuki of Yamagata University for his useful suggestions on the theory of planetary rings, Messrs. T. Segawa and S. Nakatsubo of the Construction Division of Institute of Low Temperature Science for their technical help, and Drs. F. G. Bridges and J. P. Dilley and an anonymous reviewer for critically reviewing the manuscript. The authors also thank Drs. T. Hondoh, T. Yamamoto, A. Kouchi, M. Kato, H. Narita, Y. Mizuno, K. Nishimura, and K. Kosugi for their useful comments. A portion of this research was supported by Research Fellowships from the Japan Society from the Promotion of Science for Young Scientists.

## REFERENCES

Andrews, J. P. 1930. Theory of collision of spheres of soft metal. *Phil. Mag.* **9,** 593–610.

Arakawa, M. 1995. *Experimental Study on the Dynamic Fracture and Static Flow of Ice in the Environment of Icy Planets.* Dr. thesis, University of Nagoya, Japan.

Arakawa, M., and N. Maeno 1992. Mechanical deformation of polycrystalline ice $I_h$ at temperature 100–263 K: First Report. In *Physics and Chemistry of Ice* (N. Maeno and T. Hondoh, Eds.), pp. 464–469. Univ. of Hokkaido Press, Sapporo.

Arakawa, M., and N. Maeno 1997. Mechanical strength of polycrystalline ice under uniaxial compression. *Cold Reg. Sci. Technol.* **26,** 215–229.

Araoka, K., and N. Maeno 1978. Measurements of restitution coefficients of ice. *Low Temp. Sci.* (Ser. A) **36,** 55–65. [in Japanese with English summary]

Borderies, N., P. Goldreich, and S. Tremaine 1984. Unsolved problem in planetary rings. In *Planetary Rings* (R. Greenberg and A. Brahic, Eds.), pp. 713–734. Univ. of Arizona Press, Tucson.

Bridges, F. G., A. P. Hatzes, and D. N. C. Lin 1984. Structure, stability and evolution of Saturn's rings. *Nature* **309,** 333–335.

Bridges, F. G., K. D. Supulver, D. N. C. Lin, R. Knight, and M. Zafra 1996. Energy loss and sticking mechanisms in particle aggregation in planetesimal formation. *Icarus* **123,** 422–435.

Cuzzi, J. N., J. J. Lissauer, L. W. Esposito, J. B. Holberg, E. A. Marouf, G. L. Tyler, and A. Boischot 1984. Saturn's rings: Properties and processes. In *Planetary Rings* (R. Greenberg and A. Brahic, Eds.), pp. 73–199. Univ. of Arizona Press, Tucson.

Dantl, G. 1968. Die elastichen Moduln von Eis-Einkristallen. *Phys. kondens. Materie.* **7,** 390–397.

Dilley, J. P. 1993. Energy loss in collisions of icy spheres: Loss mechanism and size-mass dependence. *Icarus* **105,** 225–234.

Dilley, J. P., and D. Crawford 1996. Mass dependence of energy loss in collisions of ice sphere: An experimental study. *J. Geophys. Res.* **90,** 9267–9270.

Gold, L. W. 1958. Some observations on the dependence of strain on stress in ice. *Can. J. Phys.* **36,** 1265–1275.

Goldreich, P., and S. Tremaine 1978. The velocity dispersion in Saturn's rings. *Icarus* **34,** 227–239.

Greenberg, R., D. R. Davise, W. K. Hartmann, and C. R. Chapman 1977. Size distribution of particles in planetary rings. *Icarus* **30,** 769–779.

Hartmann, W. K. 1978. Planet formation: Mechanism of early growth. *Icarus* **33,** 50–61.

Hatzes, A. P., F. G. Bridges, and D. N. C. Lin 1988. Collisional properties of ice spheres at low impact velocities. *Mon. Not. R. Astron. Soc.* **231,** 1091–1115.

Hatzes, A. P., F. G. Bridges, D. N. C. Lin, and S. Sachtjen 1991. Coagulation of particles in Saturn's rings: Measurements of the cohesive force of water frost. *Icarus* **89,** 113–121.

Higa, M., M. Arakawa, and N. Maeno 1996. Measurements of restitution coefficients of ice at low temperatures. *Planet. Space Sci.* **44**(9), 917–925.

Hobbs, P. V. 1974. *Ice Physics*. Clarendon Press, Oxford.

Hawkes, I., and M. Mellor 1972. Deformation and fracture of ice under uniaxial stress. *J. Glaciol.* **11,** 103–131.

Huber, M. T. 1904. Zur Theorie der Beruhrung faster elastische Korper. *Ann. Phys.* 141–144.

Johnson, K. L. 1985. *Contact Mechanics*. Cambridge Univ. Press, Cambridge, UK.

Marouf, E. A., G. L. Tyler, H. A. Zebker, R. A. Simpson, and V. R. Eshleman 1983. Particle size distributions in Saturn's rings from Voyager I radio occultation. *Icarus* **54,** 189–211.

Morton, W. B., and L. J. Close 1922. Notes on Hertz' theory of contact problems. *Phil. Mag.* **48,** 320.

Ohtsuki, K. 1992. Equilibrium velocities in planetary rings with low optical depth. *Icarus* **95,** 265–282.

Stewart, G. R., D. N. C. Lin, and P. Bodenheimer 1984. Collision-induced transport processes in planetary rings. In *Planetary Rings* (R. Greenberg and A. Brahic, Eds.), pp. 447–561. Univ. of Arizona Press, Tucson.

Supulver, K. D., F. G. Bridges, and D. N. C. Lin 1995. The coefficient of restitution of ice particles in glancing collisions: Experimental results for unfrosted surfaces. *Icarus* **113,** 188–199.

Supulver, K. D., F. G. Bridges, S. Tiscareno, J. Lievore, and D. N. C. Lin. 1997. The sticking properties of water frost produced under various ambient conditions. *Icarus* **129,** 539–554.

Timoshenko, S., and J. N. Goodier 1951. *Theory of Elasticity*, 2nd ed. McGraw-Hill, New York.

Yen, Y. C., F. Odar, A. M. Asce, and L. R. Bracy 1970. Impact of spheres on ice. *Proc. Am. Soc. Civil Eng. J. Eng. Mech. Div.* **5,** 641–652.

Zebker, H. A., E. A. Marouf, and G. L. Tyler 1985. Saturn's rings: Particle size distributions for thin later models. *Icarus* **64,** 531–548.